Measurement and Deconvolution of Glare in a microCT Scanner for In Vivo Small Animal Imaging

B. He, E.C. Frey, X. Song, T.J. Beck, S. A. Sawyer, and B.M.W. Tsui
Division of Medical Imaging Physics, Department of Radiology,
Johns Hopkins Medical Institutions, Baltimore, MD 21287-0859, USA.

***Abstract*--Recently there has been a great deal of interest in x-ray micro computed tomography (microCT) systems for in vivo small animal imaging. Although the spatial resolutions of these systems are good, the soft tissue contrast has been poor compared to human x-ray CT scanners. Many of these systems are based on phosphor screens coupled to charge coupled devices (CCD) using fiber optic tapers. The point spread function (PSF) for these systems is likely to include significant glare component. In this work we measured the glare component of the PSF of a microCT scanner developed in our laboratory. The measurements were based on the presampled edge spread function (ESF) obtained using an aluminum edge angled slightly with respect to the detector columns. The resulting ESF was fit with two Gaussian-shaped components. The wider component corresponds to the glare in the system and has a FWHM of 1.10 mm. We deconvolved this glare component from the projection data. The method was evaluated by applying the deconvolution method to projection data obtained from a mouse. The resulting projections were reconstructed using the 3D Feldkamp cone-beam reconstruction algorithm and compared to reconstructions obtained from the original projections without deconvolution. We conclude that glare deconvlution results in a modest improvement in the soft tissue contrast for small features.**

I. Introduction

Over the last several years, small animals, and particularly transgenic mice, have been widely used in genomics and cancer research. The study of small animal models for many human diseases has led to important improvement in the understanding, treatment and prevention of diseases. A good deal of research has been devoted to the development of a variety of small animal imaging systems. [1]-[5] Among these new technologies, x-ray microcomputed tomography (microCT) systems plays an important role in providing anatomical information because they can achieve images with spatial resolution better than 100 μm. These imaging systems may have a major application in *in vivo* tests and longitudinal analyses for disease studies and pharmaceutical development.

We have designed a microCT system based on a cone beam geometry and rotation of the mouse in a vertical tube. The system is constructed using an Oxford Instruments XTF5011 x-ray tube, a Medoptics CCD camera, and Velmex linear & rotational motion . The focal spot size of x-ray tube is around ~70 μm, and the x-ray power supply is remotely controlled by an Acces IO RA1216 analog/digital I/O pod. A mechanical shutter powered by a rotating solenoid controls exposure time by stopping the continuous x-ray beam. A 0.5 mm thick aluminum beam filter is used to harden the beam. The CCD imager has a pixel size of 24 μm and is coupled to a Kodak MinR phosphor by a 2:1 fiber optic taper, giving an effective pixel size of 48 μm. A detailed system description can be found in [6].

Although the microCT system has a very high bone/soft tissues contrast, the soft tissue contrast is poor without the use of contrast agents. In order to improve the soft tissue contrast, we have developed a method to measure and deconvolve the glare effect in the projection images.

II. Methods

A. Measurement of edge spread function (ESF)

In order to measure the system's resolution, we imaged an aluminum edge to measure system's edge spread function (ESF). The derivative of the ESF was taken to obtain the line spread function (LSF), and from this to point spread function (PSF) [7]-[11]

In x-ray systems, direct measurement of the point response function (PRF) is difficult. Often, the edge response fuction (ERF) is measured and the PRF derived from it. Because the

Manuscript received Oct. 29, 2003.

B. He is with the John Hopkins University, Baltimore, MD, 21287-0859, USA (telephone: 443-287-7312, e-mail: binhe@jhu.edu).
E. C. Frey is with the John Hopkins University, Baltimore, MD, 21287-0859, USA (telephone: 443-287-2426, e-mail: efrey1@jhmi.edu).
X. Song is with the John Hopkins University, Baltimore, MD, 21287-0859, USA (telephone: 443-287-7316, e-mail: xysong@jhu.edu).
T. J. Beck is with the John Hopkins University, Baltimore, MD, 21287-0859, USA (telephone: 410-955-6500, e-mail: tjbeck@jhmi.edu).
S. A. Sawyer is with the John Hopkins University, Baltimore, MD, 21287-0859, USA (telephone: 443-287-7317, e-mail: ssawyer2@jhmi.edu).
B. M. W. Tsui is with the John Hopkins University, Baltimore, MD, 21287-0859, USA (telephone: 443-287-4025, e-mail: btsui1@jhmi.edu).

resolution of the system is similar to the pixel size, measurement direct measurement of the ERF is difficult. Instead, additional samples are obtained by intentionally tilting an aluminum edged at a small angle with respect to the detector row and obtaining an x-ray transmission image. The profiles from multiple rows represent slightly shifted versions of the ERF. By shifting ERFs from multiple rows to a common center, it is possible to obtain a measurement of the ERF with very fine sampling, as shown in Figure 1.

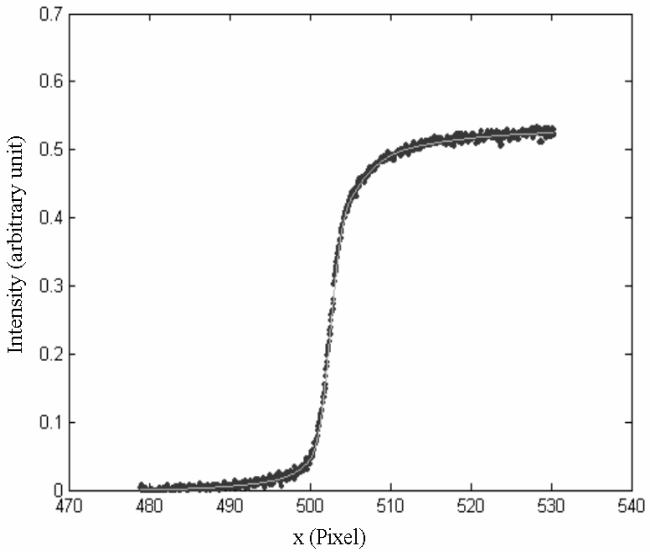

Fig. 1. A sample measured ESF. (Image matrix is 1024*1024; detector pixel size is 48 μm.) The data points represent the measured result and the line is the best lease square fit to the data using 2 error functions plus a constant.

B. Curve fitting

To characterize the ERF and separate the glare component of the PRF, we used non-linear least squares curve fitting techniques to fit the ESF with the sum of 2 error functions plus a constant, given by (1):

$$ESF(x) = a_0 + a_1 \cdot erf(\frac{x-b_1}{\sigma_1}) + a_2 \cdot erf(\frac{x-b_2}{\sigma_2}) \quad (1)$$

In equation (1), the erf is the error function given by (2):

$$erf(x) = \frac{2}{\sqrt{\pi}} \int_0^x e^{-t^2} dt \quad (2)$$

The values of the fitting parameters describing the widths and heights of the error function obtained from our ESF are:

$$a_1 = 2.29 \;\; \sigma_1 = 1.88(pixel)$$
$$a_2 = 0.98 \;\; \sigma_2 = 13.77(pixel) \quad (3)$$

The result from the best fit are shown as the line in Fig. 1.

C. Calculation of LSF

We can calculate the line resonse function function (LRF) from the ERF by taking the derivative of the fitted ESF. The resulting LRF is given by (4):

$$l(x) = 2a_1 \cdot g(x;0,\frac{\sigma_1}{\sqrt{2}}) + 2a_2 \cdot g(x;0,\frac{\sigma_2}{\sqrt{2}}) \quad (4)$$

Where $g(x;0,\frac{\sigma_1}{\sqrt{2}})$ is the Gaussian function with a mean of 0 and a standard deviation of $\frac{\sigma_1}{\sqrt{2}}$. We assume that the wider component represents glare.

The two components of the LSF are shown in Fig. 2.

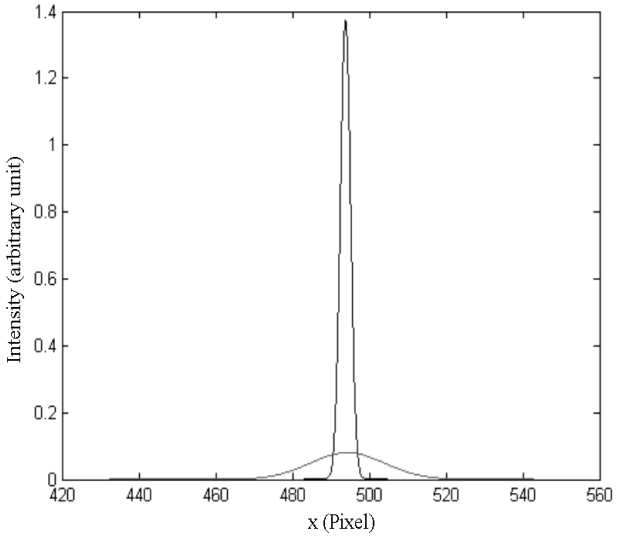

Fig. 2. The above graph shows the components of the LSF. The narrower component is assumed to be the intrinsic resolution of the system and the wider component is assumed to be the glare of the system. (pixel size is 48 μm)

By taking the one-dimensional Fourier transform of LSF, we can get system's transfer function:

$$H(|\vec{\mu}|) = 2a_1 \cdot e^{-(\pi\sigma_1\mu)^2} + 2a_2 \cdot e^{-(\pi\sigma_2\mu)^2} \quad (5)$$

D. Design of Glare Deconvolution Filter

We can model the measured projection image (m) as the convolution of true object (o) with intrinsic PRF (p) plus the function (g) representing the glare, given by (6):

$$m = o \otimes (p + g) \quad (6)$$

In frequency domain, we can deconvolve the glare component using:

$$O \cdot P = M \cdot (\frac{P}{P+G}) \quad (7)$$

Where O, P, M and G are the Fourier transforms of the true object, intrinsic PSF, measured projection image and glare function respectively.

The filtered images are the inverse Fourier transforms of $M \cdot (\frac{P}{P+G})$

Fig. 3 shows the filter (in frequency domain) that we used to deconvolve the glare component. The filtere was applied to both the measured projections and the flood image prior to log processing.

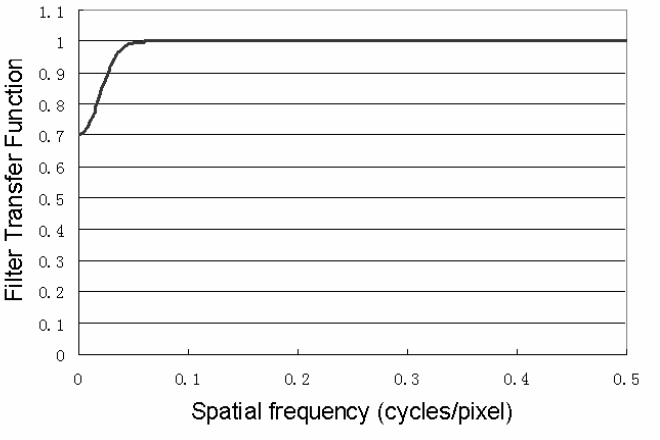

Fig. 3. The Glare Deconvolution Filter in frequency domain.

III. RESULTS

We applied the method described above to a set of mouse projection images (512*512 over 720 angles). Fig. 4 shows the comparison of the log-processed projections with and without deconvolution.

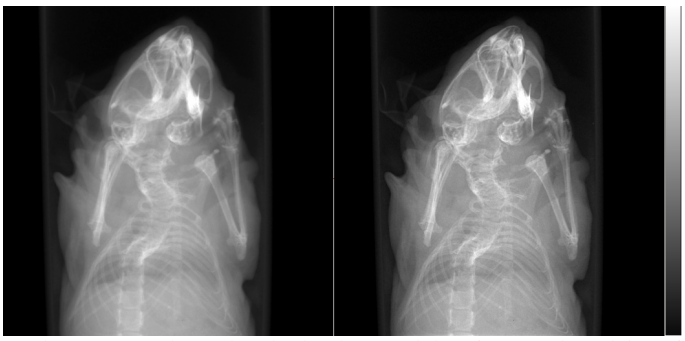

Fig. 4. Comparison of projection images. left: w/o correction, right: w/ correction. Note the improved contrast in the lung region and of small features.

Fig. 5 shows sample reconstructed images with and without prior deconvolution of the glare using Feldkamp cone beam reconstruction algorithm

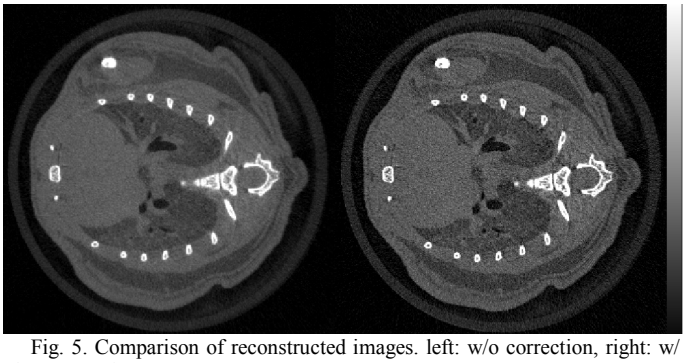

Fig. 5. Comparison of reconstructed images. left: w/o correction, right: w/ glare correction.

Glare deconvolution results in enhanced contrast, especially for small features such as those in the lungs and in the interior regions of bones. There is also an increase in high frequency image noise to to the suppression of the low frequency component of the image by the glare deconvolution filter.

IV. CONCLUSIONS

We have developed a method for measuring and deconvolving the glare component of the PSF for a microCT system. This method was evaluated by applying the deconvolution method to projection data obtained from a mouse. The method provided modest improvements in the soft tissue contrast for small features in both the projections and reconstructed images.

V. REFERENCES

[1] M. J. Paulus, S. S. Gleason, S. J. Kennel, P. R. Hunsicker and D. K. Johnson, "*High resolution X-ray computed Tomography: an emergying tool for small animal cancer research*", Neoplasia, vol. 2, Nos. 1-2, pp. 62-70, January-April 2000.

[2] M. J. Paulus, S. S. Gleason, H. Sari-Sarraf, D. K. Johnson, C. J. Flotz, D. W. Austin, M. e. Easterly, E. J. Michaud, M. S. Dhar, P. R. Hunsicker, J. W. Wall and M. Schell, "*High-resolution x-ray CT screening of mutant mouse models*", the SPIE International Symposium on Biomedical Optics, San Jose, January 22-27, 2000.

[3] D. W. Holdsworth, M. Drangova and A. Fenster, "*A high-resolution XR-based quantitative volume CT scanner*", Medical Phsyics, vol. 20, No. 2, Pt. 1, Mar/Apr 1993.

[4] P. Ruegsegger, B. Koller and R. Muller, "*A microtomography system for the nondestructive evaluation of bone architecture*", Calcified Tissue International, 58:24-29, 1996.

[5] X. Song, E. C. Frey, and B.M.W. Tsui, "*Development and evaluation of a microCT system for small animal imaging*", Conference Record of 2001 IEEE Nuclear Science Symposium and Medical Imaging Conference, San Diego, CA, USA, vol. 3, pp. 1600-1604, Oct. 2001.

[6] M. Khodaverdi, F. Pauly, S. Weber, G. Schroder, K. Ziemons, R. Sievering, and H. Halling, "*Preliminary studies of a microCT for a combined small animal PET/CT scanner.*" Conference Record of the 2001 IEEE Nuclear Science Symposium and Medical Imaging Conference, San Diego, CA, USA, vol. 3, pp. 1605 -1606, Oct. 2001.

[7] R. A. Jones, "*An automated technique for deriving MTF's from edge traces*", Photograph. Sci. Eng. 11, 102–106 (1967).

[8] J. C. Dainty and R. Shaw, "*Image Science*", Academic, New York, 1974.

[9] I. A. Cunningham and A. Fenster, "*A method for modulation transfer function determination from edge profiles with correction for finiteelement differentiation*", Med. Phys. 14, 533–537 (1987).

[10] I. A. Cunningham and B. K. Reid, "*Signal and noise in modulation transfer function determinations using the slit, wire, and edge techniques*", Med. Phys. 19, 1037–1044 (1992).

[11] E. Samei and M. J. Flynn, "*A method for measuring the presampled MTF of digital radiographic systems using an edge test device*", Med. Phys. 25, 102–113 (1998).

[12] J. A. Seibert, O. Nalcioglu, and W. Roeck, "*Characterization of the veiling glare PSF in x-ray image intensified fluoroscopy*", Med. Phys. 11, 172–179 (1984)